SOFT ROBOTICS
Volume 00, Number 00, 2019
© Mary Ann Liebert, Inc.
DOI: 10.1089/soro.2019.0060

Single-Input Control of Multiple Fluid-Driven Elastic Actuators Via Interaction Between Bistability and Viscosity

Eran Ben-Haim,[1] Lior Salem,[2] Yizhar Or,[1,2] and Amir D. Gat[1,2]

Abstract

A leading concept in soft robotics actuation, as well as in microfluidics applications such as valves in lab-on-a-chip devices, is applying pressurized flow in cavities embedded within elastic bodies. Generating complex deformation patterns typically requires control of several inputs, which greatly complicates the system's operation. In this study, we present a novel method for *single-input control* of a serial chain of *bistable* elastic chambers connected by thin tubes. Controlling a single flow rate at the chain's inlet, we induce an irreversible sequence of transitions that can reach any desired state combination of all bistable elements. Mathematical formulation and analysis of the system's dynamics reveal that these transitions are enabled, thanks to bistability combined with pressure lag induced by viscous resistance. The results are demonstrated through numerical simulations combined with experiments for chains of up to five chambers, using water-diluted glycerol as the injected fluid. The proposed technique has a promising potential for development of sophisticated soft actuators with minimalistic control.

Keywords: bistability, minimalistic control, fluid-driven actuation

Introduction

Soft robotics is a rapidly emerging field where large continuous deformations and compliant interaction with external loads or environment are combined and harnessed for various applications of tactile manipulation, locomotion in unstructured environments, and biomedical applications.[1,2] A leading effective method of soft actuation is based on an elastic structure containing embedded network of cavities filled with fluid, while controlling pressures or flow rates at the network's inlets.[3,4] The recent study[5] shows promising biomedical application of a soft robot for colonoscopy, which utilizes a double-balloon system for achieving inchworm-like crawling while bracing against colonic walls.

Pressure control of multiple liquid-filled elastic chambers is also commonly used to actuate onboard valves in the field of lab-on-a-chip devices, in which it is often required to dynamically change the geometry of internal microfluidic networks.[6–8] Generating and coordinating complex deformation patterns with such actuators (Tolley *et al.*[9]) or microvalves (Mosadegh *et al.*[10]) typically requires control of several inputs, which greatly complicates the system's operation.

An additional feature exploited for efficient elastic actuation is using *bistability* of flexible elements for inducing rapid ''jumps'' between different stable equilibrium states due to excitation by minimal input.[11,12] Several works study the behavior of a serial chain of bistable elastic elements, where actuation can either be thermal,[13,14] electrical,[15,16] or tension forces.[17–19] In the case of fluidic actuation, several works study variations of the well-known ''two-balloon system,'' whereas others study networks of multiple connected chambers. Importantly, in many of these works, each element has its own control input for inducing transitions between its bistable states.[15,16,20] Other works consider systems with a single control input[13,14,17,19] or no input[21,22] (network with closed fluid domain), but do not allow for arbitrary control of transitions.

The study[23] achieved a desired specific reversible sequence of state transitions of the bistable elements due to preplanned mechanical tuning. The study[24] has demonstrated crawling locomotion using an irreversible gait in a robot composed of serially connected bistable balloons, for potential biomedical applications. The recent study[25] uses a similar two-balloon system with pretuned stiffness asymmetry as a

---

[1] Faculty of Mechanical Engineering, Technion—Israel Institute of Technology, Haifa, Israel.
[2] Technion Autonomous Systems Program, Technion—Israel Institute of Technology, Haifa, Israel.

single-input pneumatic two-joint actuator for achieving quasistatic locomotion of a quadruped robot. Importantly, the studies[24,25] were both limited to achieving a specific predetermined gait of cyclic transition sequence and did not include systematic stability analysis of the system's states and possible transitions.

In this study, we present a novel method for achieving irreversible sequences of transitions between any arbitrary equilibrium states for a serial chain of bistable elastic chambers connected by thin tubes, using a single input of inlet flow rate. We present mathematical formulation of the system's dynamics and analyze its stability and transitions. The results are demonstrated through numerical simulations combined with laboratory experiments for chains of up to five chambers, using fluids of different viscosities. Schematic picture of our experimental setup and its illustration with notations are shown in Figure 1a and b, respectively.

Formulation of Elastic Bistability

We begin by introducing the main effect that enables state transitions in a pressurized thin hyperelastic chamber, namely its *bistability*, which induces multiple solutions of possible volumes for a given pressure. For an ideally spherical chamber with stress-free radius r_0 and shell thickness d_0, let $\lambda = r/r_0$ denote the *relative stretch* of the chamber, where r is its varying radius. For a thin-shelled chamber made of incompressible hyperelastic isotropic material such as rubber, finite elasticity theory dictates a known form of elastic strain energy density[21,27–29]:

$$\psi(\lambda) = \sum_{k=1}^{K} \frac{s_k}{\alpha_k}(2\lambda^{\alpha_k} + \lambda^{-2\alpha_k} - 3), \tag{1}$$

where the powers α_k are inherent to any specific constitutive law, whereas the coefficients s_k take empirical values that depend on material properties. The isotropic pressure in the shell can then be obtained from Equation (1) as (cf. Beatty[30]):

$$p = \frac{d_0}{r_0}\frac{1}{\lambda^2}\cdot\frac{d\psi}{d\lambda} = 2\frac{d_0}{r_0}\sum_{k=1}^{K} s_k(\lambda^{\alpha_k-3} - \lambda^{-2\alpha_k-3}). \tag{2}$$

Using the chamber's volume $V = \frac{4}{3}\pi r^3$, the pressure in Equation (2) can also be written in terms of V as

$$p\, :\, = F(V) = 4\pi d_0 r_0^2 \frac{d\psi}{dV}. \tag{3}$$

Using a calibration experiment with a single chamber, Figure 1c shows the measured stretch–pressure characteristic curve. The best-fit model for this particular curve is Ogden's law.[26] In Ogden's model, Equation (1) contains three terms in the elastic strain energy density ($K = 3$), corresponding to powers of $\alpha_1 = 1.3$, $\alpha_2 = 5$, $\alpha_3 = -2$ in Equation (2). This curve appears in dashed line in Figure 1c. The Supplementary Data contains details of the calibration experiment and the fitting process, as well as comparison with other known elasticity laws.[21,27,28,30] The characteristic curve $p(\lambda)$ in Figure 1c has a local maximum point at (λ_A, p_A) and a local minimum point at (λ_B, p_B). For the intermediate range of pressures $p \in (p_A, p_B)$, there exist multiple solutions of stretch λ. We denote the stretch ranges $\lambda < \lambda_A$ and $\lambda > \lambda_B$ as "small" and "big" chambers, respectively, which are also represented by binary states "0" and "1." Analyzing the strain energy function $\psi(\lambda)$ in Equation (1), it can be proven that these upper and lower solution branches of $p(\lambda)$ are stable equilibria and satisfy $d^2\psi/d\lambda^2 > 0$. Conversely, the intermediate branch $\lambda \in (\lambda_A, \lambda_B)$ is an unstable solution satisfying $d^2\psi/d\lambda^2 < 0$. This is precisely the bistability phenomenon, which is exploited in this study for controlled transitions of between combinations of the chambers' binary states.

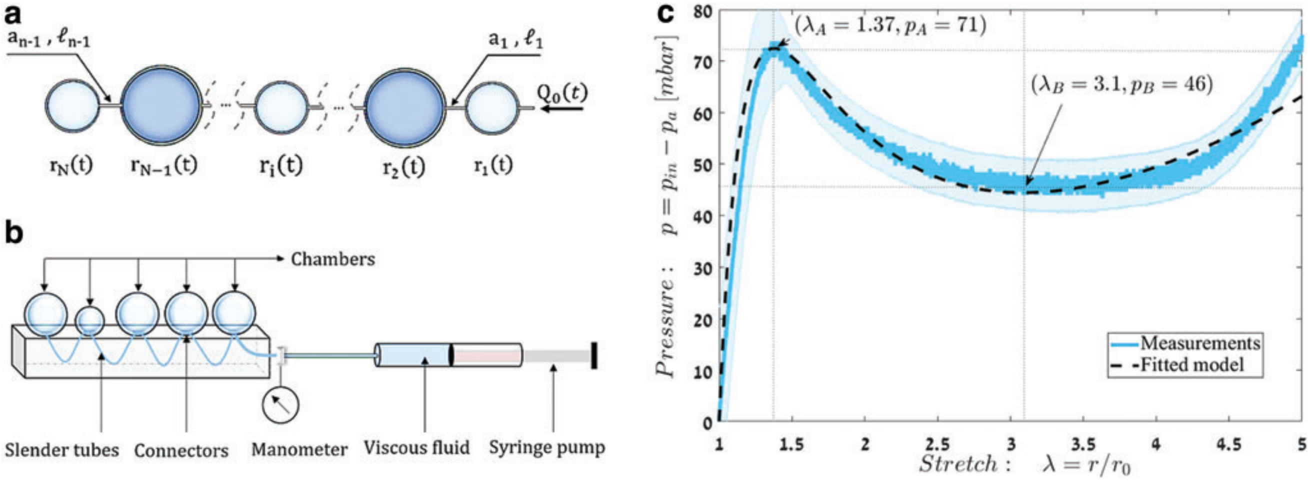

FIG. 1. **(a)** Illustration of the system with notation. **(b)** Schematic picture of a serial chain of elastic chambers with a single inlet. **(c)** Characteristic stretch–pressure curve of a single elastic chamber obtained from experimental measurements (*solid line*) and the best-fit theoretical curve (*dashed line*) using Ogden's law.[26] The shaded area enveloping the solid curve denotes one standard deviation around mean value. Fitting values to Equation (2) were obtained as $s_1 = 172.04[mBar]$, $s_2 = 2.59[mBar]$, $s_3 = 1.98[mBar]$, resulting in root-mean-square (RMS) error of $28.67[mBar]$ and $R^2 = 0.9862$. Color images are available online.

Analysis of Multichamber System

We now consider a serial chain of N identical chambers connected by thin circular tubes, as shown in Figure 1a. The system is filled by incompressible Newtonian fluid with density ρ and viscosity μ. We denote Q_i as the mass flow rate at the tube connecting the chambers i and $i+1$, where the only controlled input is the time-varying mass flow rate $Q_0(t)$ at the inlet of the first chamber. Each tube has radius of a_i and length l_i. Denoting the volume of the ith chamber as $V_i=\frac{4}{3}\pi(r_0\lambda_i)^3$, mass rate balance for each chamber gives:

$$\rho\frac{dV_i}{dt}=4\rho\pi r_0^3\lambda_i^2\frac{d\lambda_i}{dt}=Q_{i-1}-Q_i\ for\ i=1\dots N. \qquad (4)$$

The fact that the chain has no outlet is represented by the end condition $Q_N=0$. We assume steady and fully developed axisymmetric flow in the tubes, with uniform pressure gradient. Neglecting end effects, this gives a linear relation between viscous flow rate and pressure difference at the ith tube as

$$Q_i=\frac{p_i-p_{i+1}}{R_i}, \qquad where\ R_i=\frac{8\mu l_i}{\pi\rho a_i^4}. \qquad (5)$$

Finally, assuming quasistatic equilibrium and uniform pressure at each chamber implies that the fluid pressures p_i at the ith chamber is equal to the pressure in the chamber's shell and satisfies the characteristic relation $p_i=F(V_i)$, where the function $F(V)$ is given in Equation (3). Substituting into Equation (5) gives

$$Q_i=\frac{F(V_i)-F(V_{i+1})}{R_i}. \qquad (6)$$

The assumptions listed earlier ensure that this simplified model of the system's dynamics remains valid. In general, they hold when the tubes are sufficiently slender $a_i \ll l_i$ and when the inlet flow rate Q_0 is sufficiently slow. Explicit formulation and further discussion of these assumptions, including scaling analysis, appear in the Supplementary Data. Substituting Equations (6) into (4) gives a nonlinear coupled system of N first-order differential equations that govern the dynamic evolution of chambers' volumes $V_i(t)$ under the single input $Q_0(t)$. Equilibrium states of the system under zero input $Q_0=0$ for which the total volume is conserved impose that all chambers' pressures are equal $p_1=p_2\dots=p_N$. For a given total volume $V_{tot}=V_1+\dots+V_N$, this condition may have multiple solutions due to bistability of the stretch–pressure relation in Equation (2), see Figure 1c. Assuming slow changes in the total volume, the system moves quasistatically along equilibrium solutions. That is, setting zero input $Q_0=0$, the system simply stops at an equilibrium state. However, any small nonzero input $Q_0(t)$ still induces small deviations from equilibrium, and thus divergence from, or convergence to, solutions of static equilibrium is determined by their *dynamic stability*. Stability analysis of the system's equilibria is detailed in the Supplementary Data. For the case of two chambers, the condition for stability of an equilibrium state with volumes (V_1^e, V_2^e) is given by

$$\left.\frac{dF}{dV}\right|_{V_1^e}+\left.\frac{dF}{dV}\right|_{V_2^e} > 0. \qquad (7)$$

For the case of three chambers, the stability condition (Eq. 7) still holds, and is augmented by the additional condition

$$\left.\frac{dF}{dV}\right|_{V_1^e}\cdot\left.\frac{dF}{dV}\right|_{V_2^e}+\left.\frac{dF}{dV}\right|_{V_1^e}\cdot\left.\frac{dF}{dV}\right|_{V_3^e}+\left.\frac{dF}{dV}\right|_{V_2^e}\cdot\left.\frac{dF}{dV}\right|_{V_3^e} > 0. \qquad (8)$$

Extension to general case of multiple chambers appears in the Supplementary Data.

To illustrate the concepts of multiple equilibrium solution branches and their dynamic stability, we first consider the two-chamber system $N=2$. A plot of the equilibrium solution branches in the plane of stretches (λ_1,λ_2) under $Q_0=0$ is shown in Figure 2. Using the stability condition (Eq. 7),

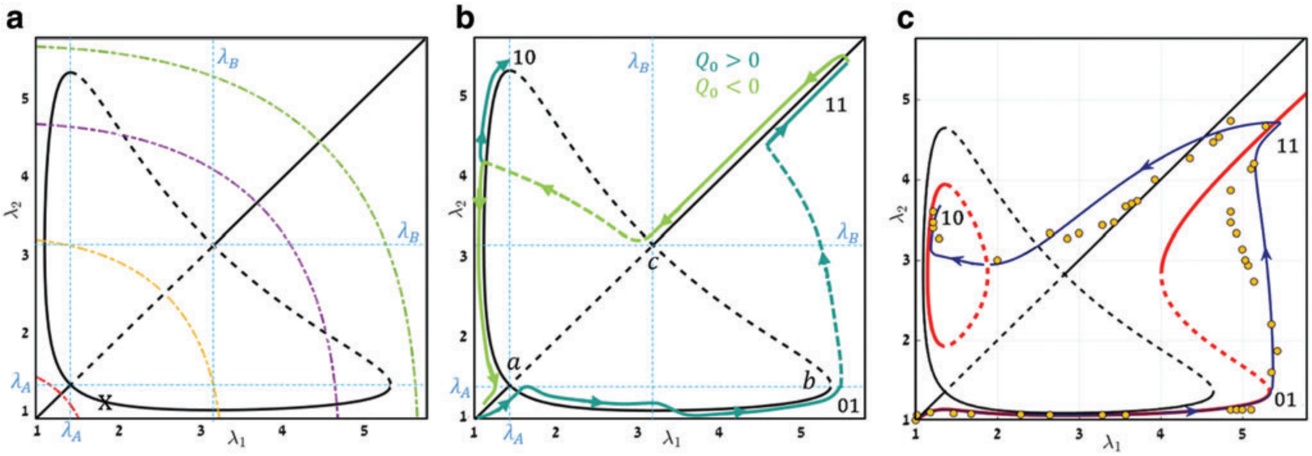

FIG. 2. **(a)** Equilibrium curves of the two-chamber system in (λ_1,λ_2) plane. *Solid curves* are stable branches and *dashed curves* are unstable ones. *Dash-dotted cubic curves* are constant total volume $\lambda_1^3+\lambda_2^3=Const$. **(b)** Solution trajectories of numerical simulation, overlaid on the branches of equilibrium curves. **(c)** Results of experimental measurements as *circles* in (λ_1,λ_2)-plane. *Black lines* are theoretical curves of equilibrium $p_1=p_2$ (*solid*, stable; *dashed*, unstable). *Red thick lines* are equilibrium curves of asymmetric chambers with $c=0.3$ showing good agreement with experimental measurements. Color images are available online.

solution branches of stable equilibria are marked by solid lines, whereas branches of unstable equilibria are marked by dashed lines. Importantly, stability condition for the system's equilibria is fundamentally different from stability of a single chamber based on its elastic potential ψ in Equation (1). For example, the point marked by ''$\times$'' on Figure 2a is a stable equilibrium state even though chamber 1 seems to be in an ''unstable'' solution branch $\lambda_1 \in (\lambda_A, \lambda_B)$. The dash-dotted arcs in Figure 2a denote curves of constant total volume $\lambda_1^3 + \lambda_2^3 = const$. When the system is initially placed out of equilibrium with $Q_0 = 0$, the solution moves along these curves and converges toward stable equilibrium branches. This plot can also provide an elegant explanation to the counterintuitive behavior of the well-known two-balloon experiment,[21,31] see details in the Supplementary Data.

Next, we consider a scenario where the system undergoes irreversible sequence of transitions between the chambers' combined states, while being controlled by a single input of flow rate $Q_0(t)$. The chosen input is piecewise constant. Figure 2b shows the system's trajectory in (λ_1, λ_2)-plane, overlaid on the equilibrium curves. The plots show how the system goes through the irreversible sequence of states $00 \rightarrow 01 \rightarrow 11 \rightarrow 10 \rightarrow 00$, where the rightmost digit corresponds to the state of chamber 1. These state transitions are made possible by exploiting the following two key effects. First, when the state trajectory follows a stable branch and reaches a point where it becomes unstable, as in points ''a,b,c'' in Figure 2b, the trajectory rapidly ''jumps'' and converges to a stable branch, moving very close to a cubic arc of constant total volume, $\lambda_1^3 + \lambda_2^3 = const$. The second key effect, which dictates the ''choice'' of the direction to which the solution converges after loss of stability, is explained as follows. Under small nonzero input, the sign of Q_0 combined with the current stretches $\lambda_i(t)$ dictate the sign of nonequilibrium pressure difference $\Delta p = p_2 - p_1 \neq 0$. This results in small deviation of the state trajectory from an equilibrium curve in a specific direction, as seen in Figure 2b. Thus, when the trajectory approaches bifurcation points ''a,c,'' deviations from the symmetry line $\lambda_1 = \lambda_2$ imposed by the sign of Δp dictate different ''choices'' of converging toward particular stable branches. Figure 3a shows time plot of the input $Q_0(t)$, which represents a slow process of inflation followed by

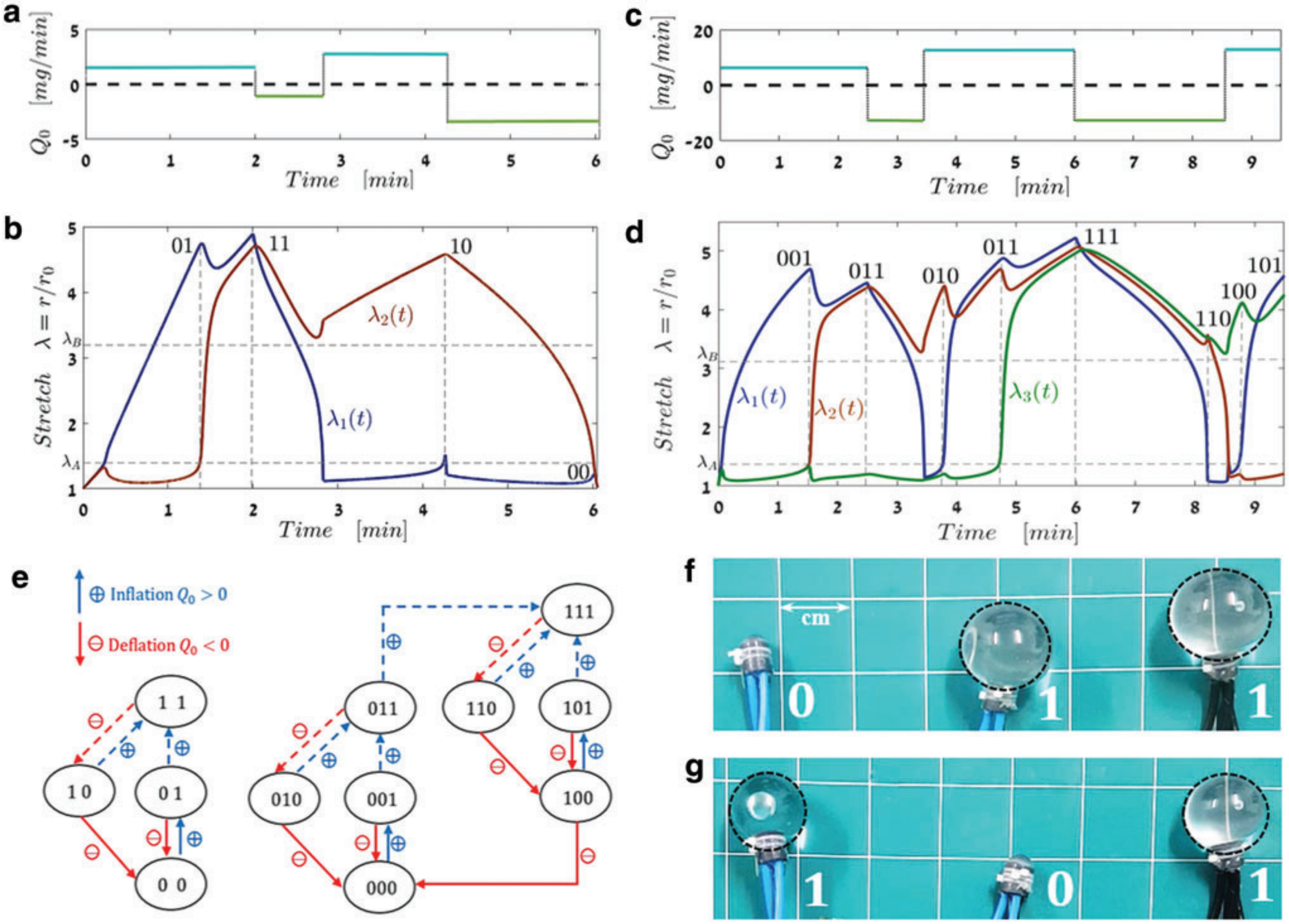

FIG. 3. **(a)** Time plot of inlet flow $Q_0(t)$ for inflation and deflation in case of two chambers. **(b)** Time plots of chambers' stretches $\lambda_i(t)$ obtained by numerical integration of the nonlinear dynamical system with $N = 2$ chambers. **(c)** Time plot of inlet flow $Q_0(t)$ in case of three chambers. **(d)** Time plots of chambers' stretches $\lambda_i(t)$ with $N = 3$ chambers. **(e)** State transitions graph for systems of two and three chambers (*left* for $N = 2$ and *right* for $N = 3$), *dashed arrows* represent transitions of ''jumps'' due to stability loss of previous state. **(f, g)** Snapshots from experiment with $N = 3$ chambers, showing example of two different binary states ''011'' and ''101.'' Color images are available online.

deflation. Figure 3b shows time plots of the two stretches $\lambda_1(t)$ and $\lambda_2(t)$, which are obtained through numerical integration of the two-chamber system of differential equations.

These principles can be generalized to a serial chain of N chambers, and induce a graph of possible transitions between binary states, achievable by using either inflation $Q_0 > 0$ or deflation $Q_0 < 0$. As an example, we present numerical simulations for chains of three and five chambers, and demonstrate generating a desired sequence of states. Time plots of the chosen input flow rate $Q_0(t)$ and the stretches $\lambda_i(t)$ are shown in Figure 3c and d, and in Figure 4a. Transition graphs for $N = 2$ and $N = 3$ are shown in Figure 3e, whereas graphs for $N = 4, 5$ appear in the Supplementary Data. Importantly, implementation of such ordered sequences of single-input state transitions does not depend on the particular details of the stretch–pressure characteristic curve in Equation (2) nor on specific pressure–flow rate relation (Eq. 4). The only two necessary ingredients are the bistable form as shown in Figure 1b, combined with existence of nonequilibrium pressure deviation Δp induced by viscous resistance of the tubes.

Experiments

Our experimental setup of $N = \{2, 3, 5\}$ elastic chambers connected serially through thin semiflexible tubes. The chambers were made of industrial latex, and were cut from Durex® condoms (except for some illustrative two-balloon experiments with commercial sausage balloons). The hyperelastic stretch–pressure relation of a single chamber has been measured and numerically fitted to Ogden's law, see Figure 1c. The inlet is connected to a flow controller "*neMESYS XL 7000N*" of Cetoni® through a tube of length $l_0 = 0.5m$ and circular cross section of radius $a_0 = 10mm$. The tubes connecting all other chambers have equal lengths of $l_i = 0.4m$ and radius of $a_i = 1.5mm$, for $i = 1 \dots N$. Custom-made connectors between chambers and tubes were made from *Smooth-On Dragon-Skin* by casting it into 3D-printed molds, see Supplementary Data for details. Most of the experiments were conducted with water-diluted glycerol of viscosity $\mu \approx 1.2[Pa \cdot s]$ and density $\rho \approx 1.26[g/cm^3]$. The high viscosity was exploited for increased lag and pressure differences Δp between consecutive chambers, which helps

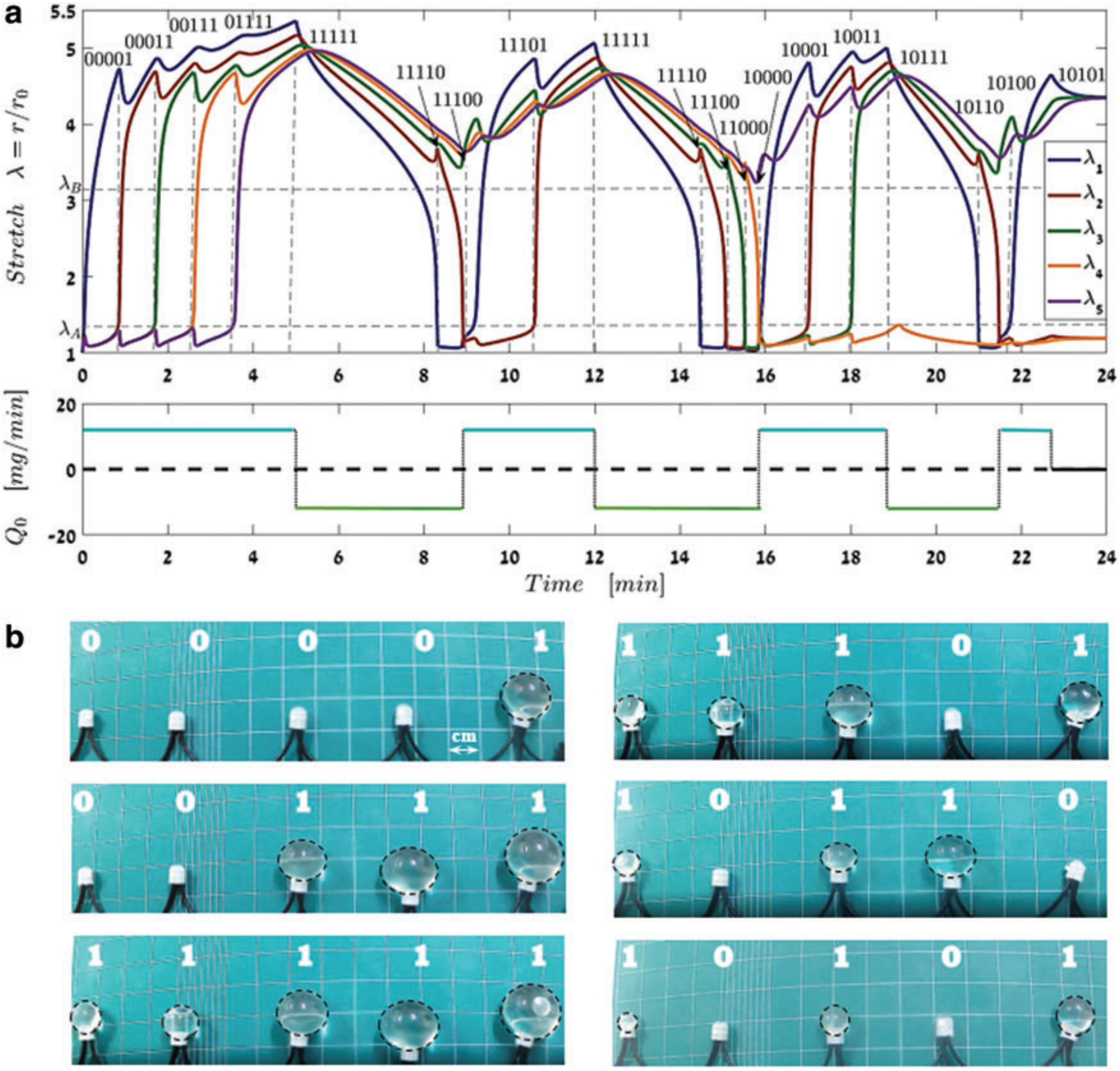

FIG. 4. (**a**) Time plots of $Q_0(t)$ and $\lambda_i(t)$ for numerical simulation of the systems with $N = 5$ chambers. Here we present 16 different binary states yielded by single input $Q_0(t)$ that plotted below this graph. (**b**) Snapshots of experiment with $N = 5$ chambers showing sequence of transitions between binary states. Color images are available online.

in emphasizing the effect of selective irreversible state transitions. More details on the experiments and measurements, as well as video movie files of experiments appear in the Supplementary Data. Figure 2c shows state trajectory in the plane of (λ_1, λ_2) obtained from measurements of experiment with $N = 2$. The experiment shows irreversible state transition sequence of $00 \rightarrow 10 \rightarrow 11 \rightarrow 01$, as shown in the simulations earlier (Figs. 2b and 3b). The deviation between experimental measurements and theoretical equilibrium curves (overlaid on the plot in black) can be explained by imperfections of asymmetry between the two chambers. This can be captured in the theoretical model by assuming small differences in shell thickness d_0 and stress-free radius r_0 between the two chambers, which are manifested by replacing the elasticity relations in Equation (2) with $p_1 = F(\lambda_1)$ and $p_2 = (1 + c)F(\lambda_2)$, where c is a small factor representing this asymmetry. The red curves on the plot in Figure 2c represent the asymmetric equilibrium branches $p_1 = p_2$ under $c = 0.3$. It can be seen that introducing this simple asymmetry factor into the model improves quantitative agreement with the experimental measurements. Finally, we present results of experiments with $N = 3$ and $N = 5$ chambers. Snapshots of representative binary states of the system are shown in Figure 3f and 3g, and in Figure 4b. A video movie of a sequence of transitions between 16 states for $N = 5$ appears in the Supplementary Data.

Concluding Discussion

In summary, we have presented a method for inducing irreversible sequences of state transitions in a serially connected chain of fluid-filled chambers using a single input of flow rate. The method exploits bistability of equilibrium states for hyperelastic thin shells, as well as pressure differences induced by viscous effects. We presented theoretical analysis, numerical simulations, and experiments with inflatable balloons. This method enables overcoming the complexity of controlling each element using a separate input, and thus has a promising potential for creating minimal-control soft actuators that can be utilized in several applications of robotics and biomedicine. The concept has been already proven useful for pneumatic actuators of legged robots achieving quasistatic locomotion.[25] In addition, it has promising potential for inchworm-like crawling of a two-balloon system,[24] which has recently been utilized for a colonoscopy device.[5]

The proposed concept is still limited in terms of achievable sequences of state transitions, as illustrated in the transition graphs. Pretuned asymmetry in stiffness of different elements can be used to impose prescribed order of transitions, as demonstrated in Overvelde *et al.*[23] and Gorissen *et al.*[25] Other possible ways for increasing the versatility of achievable state transitions are changing the topology of flow connection between chambers by adding junctions and parallel connections with varying resistances, as well as adding mechanical coupling of forces applied between different elements, and against environment or external loads. Systematic investigation of such configurations of fluid networks of bistable elements is still an open challenge.

Finally, our theoretical model uses the simplifying assumptions of incompressible viscous fluid and quasistatic motion with fully developed uniform pressure in the chambers, see detailed analysis in the Supplementary Data. Relaxing the quasistatic assumption, we currently work on analysis of the transient dynamics of inflating a single axisymmetric (hyper) elastic chamber. As for relaxing the assumption of incompressible fluid, although we were able to conduct successful experiments of state transitions also with air-inflated chambers, extending the theoretical formulation to ideal compressible gas, which complicates also the stability analysis, is relegated to future study.

Author Disclosure Statement

No competing financial interests exist.

Funding Information

This research has been supported by Israel Ministry of Science and Technology, under grant number 3-14418.

Supplementary Material

Supplementary Data

References

1. Aguilar J, Zhang T, Qian F, *et al.* A review on locomotion robophysics: the study of movement at the intersection of robotics, soft matter and dynamical systems. Rep Prog Phys 2016;79:110001.
2. Rus D, Tolley MT. Design, fabrication and control of soft robots. Nature 2015;521:467.
3. Polygerinos P, Correll N, Morin SA, *et al.* Soft robotics: review of fluid-driven intrinsically soft devices; manufacturing, sensing, control, and applications in human-robot interaction. Adv Eng Mater 2017;19:1700016.
4. Marchese AD, Katzschmann RK, Rus D. A recipe for soft fluidic elastomer robots. Soft Robot 2015;2:7–25.
5. Manfredi L, Capoccia E, Ciuti G, *et al.* A soft pneumatic inchworm double balloon (SPID) for colonoscopy. Sci Rep 2019;9:11109.
6. Unger MA, Chou H-P, Thorsen T, *et al.* Monolithic microfabricated valves and pumps by multilayer soft lithography. Science 2000;288:113–116.
7. Thorsen T, Maerkl SJ, Quake SR. Microfluidic large-scale integration. Science 2002;298:580–584.
8. Desai AV, Tice JD, Apblett CA, *et al.* Design considerations for electrostatic microvalves with applications in poly (dimethylsiloxane)-based micro fluidics. Lab Chip 2012;12:1078–1088.
9. Tolley MT, Shepherd RF, Mosadegh B, *et al.* A resilient, untethered soft robot. Soft Robot 2014;1:213–223.
10. Mosadegh B, Kuo C-H, Tung Y-C, *et al.* Integrated elastomeric components for autonomous regulation of sequential and oscillatory flow switching in micro fluidic devices. Nat Phys 2010;6:433.
11. Rothemund P, Ainla A, Belding L, *et al.* A soft, bistable valve for autonomous control of soft actuators. Sci Robot 2018;3:eaar7986.
12. Zhakypov Z, Mori K, Hosoda K, *et al.* Designing minimal and scalable insect-inspired multilocomotion millirobots. Nature 2019;571:381–386.
13. Chen T, Shea K. An autonomous programmable actuator and shape reconfigurable structures using bistability and shape memory polymers. 3D Print Addit Manuf 2018;5: 91–101.

14. Che K, Yuan C, Qi HJ, *et al*. Viscoelastic multistable architected materials with temperature-dependent snapping sequence. Soft Matter 2018;14:2492–2499.
15. Li T, Keplinger C, Baumgartner R, *et al*. Giant voltage-induced deformation in dielectric elastomers near the verge of snap-through instability. J Mech Phys Solids 2013;61: 611–628.
16. Hines L, Petersen K, Sitti M. Inflated soft actuators with reversible stable deformations. Adv Mater 2016;28:3690–3696.
17. Benichou I, Faran E, Shilo D, *et al*. Application of a bi-stable chain model for the analysis of jerky twin boundary motion in NiMnGa. Appl Phys Lett 2013;102: 011912.
18. Puglisi G, Truskinovsky L. Mechanics of a discrete chain with bi-stable elements. J Mech Phys Solids 2000;48:1–27.
19. Cohen T, Givli S. Dynamics of a discrete chain of bi-stable elements: a biomimetic shock absorbing mechanism. J Mech Phys Solids 2014;64:426–439.
20. Fei Y, Pang W. Analysis on nonlinear turning motion of multi-spherical soft robots. Nonlinear Dyn 2017;88: 883–892.
21. MÃijller I, Strehlow P. Rubber and Rubber Balloons: Paradigms of Thermodynamics, Volume 637. New York, NY: Springer Science & Business Media, 2004.
22. Dreyer W, MÃijller I, Strehlow P. A study of equilibria of interconnected balloons. Quart J Mech Appl Math 1982;35: 419–440.
23. Overvelde JT, Kloek T, DâĂZhaen JJ, *et al*. Amplifying the response of soft actuators by harnessing snap-through instabilities. Proc Natl Acad Sci USA 2015;112:10863–10868.
24. Glozman D, Hassidov N, Senesh M, *et al*. A self-propelled inflatable earthworm-like endoscope actuated by single supply line. IEEE Trans Biomed Eng 2010;57:1264–1272.
25. Gorissen B, Milana E, Baeyens A, *et al*. Hardware sequencing of inflatable nonlinear actuators for autonomous soft robots. Adv Mater 2019;31:1804598.
26. Ogden RW. Large deformation isotropic elasticity—on the correlation of theory and experiment for incompressible rubberlike solids. Proc R Soc Lond A 1972;326:565–584.
27. Treloar LRG. The Physics of Rubber Elasticity. Oxford, NY: Oxford University Press, 1975.
28. Holzapfel GA. Nonlinear solid mechanics: a continuum approach for engineering science. Meccanica 2002;37: 489–490.
29. Vandermarlière J. On the inflation of a rubber balloon. Phys Teacher 2016;54:566–567.
30. Beatty MF. Topics in finite elasticity: hyperelasticity of rubber, elastomers, and biological tissues—with examples. Appl Mech Rev 1987;40:1699–1734.
31. Weinhaus F, Barker W. On the equilibrium states of interconnected bubbles or balloons. Am J Phys 1978;46: 978–982.

Address correspondence to:
Yizhar Or
Faculty of Mechanical Engineering
Technion—Israel Institute of Technology
Haifa 3200003
Israel

E-mail: izi@technion.ac.il